LEGIBILITY NOTICE

A major purpose of the Technical Information Center is to provide the broadest dissemination possible of information contained in DOE's Research and Development Reports to business, industry, the academic community, and federal, state and local governments.

Although a small portion of this report is not reproducible, it is being made available to expedite the availability of information on the research discussed herein.

CONF-8709107--1

Los Alamos National Laboratory is operated by the University of California for the United States Department of Energy under contract W-7405-ENG-36

LA-UR--87-2251

DE87 011727

TITLE NUMERICAL PREDICTIONS OF EML SYSTEM PERFORMANCE

AUTHOR(S) Norman M. Schnurr, Jerry F. Kerrisk, and Rich F. Davidson

SUBMITTED TO Proceedings of the Fifth US Army Symposium on Gun Dynamics
Rensselaerville, New York, September 23-25, 1987

DISCLAIMER

LOS ALAMOS Los Alamos National Laboratory
Los Alamos, New Mexico 87545

NUMERICAL PREDICTIONS OF EML SYSTEM PERFORMANCE

N. M. Schnurr, J. F. Kerrisk, and R. F. Davidson
Los Alamos National Laboratory
P.O. Box 1663
Los Alamos, New Mexico 87545

ABSTRACT

The performance of an electromagnetic launcher (EML) depends on a large number of parameters, including the characteristics of the power supply, rail geometry, rail and insulator material properties, injection velocity, and projectile mass. EML system performance is frequently limited by structural or thermal effects in the launcher (railgun). A series of computer codes has been developed at the Los Alamos National Laboratory to predict EML system performance and to determine the structural and thermal constraints on barrel design. These codes include FLD, a two-dimensional electrostatic code used to calculate the high-frequency inductance gradient and surface current density distribution for the rails; TOPAZRG, a two-dimensional finite-element code that simultaneously analyzes thermal and electromagnetic diffusion in the rails; and LARGE, a code that predicts the performance of the entire EML system. The NIKE2D code, developed at the Lawrence Livermore National Laboratory, is used to perform structural analyses of the rails.

These codes have been instrumental in the design of the Lethality Test System (LTS) at Los Alamos, which has an ultimate goal of accelerating a 30 g projectile to a velocity of 15 km/s. The capabilities of the individual codes and the coupling of these codes to perform a comprehensive analysis is discussed in relation to the LTS design. Numerical predictions are compared with experimental data and presented for the LTS prototype tests.

NUMERICAL PREDICTIONS OF EML SYSTEM PERFORMANCE

N. M. Schnurr, J. F. Kerrisk, and R. F. Davidson
Los Alamos National Laboratory
P.O. Box 1663
Los Alamos, New Mexico 87545

INTRODUCTION

Electromagnetic launchers or railguns are devices that accelerate projectiles to high velocities by the interaction of an electric current and a magnetic field [1,2]. A schematic diagram of a railgun is shown in Fig. 1. The basic elements include two parallel stationary conductors (rails) that are bridged by a moving armature. When the main switch is thrown, the capacitor bank discharges, a voltage is applied across the rails, and an electric current flows down one rail, through the armature, and back through the other rail. The current in the rails gives rise to a magnetic field that interacts with the armature current to cause a Lorenz force on the

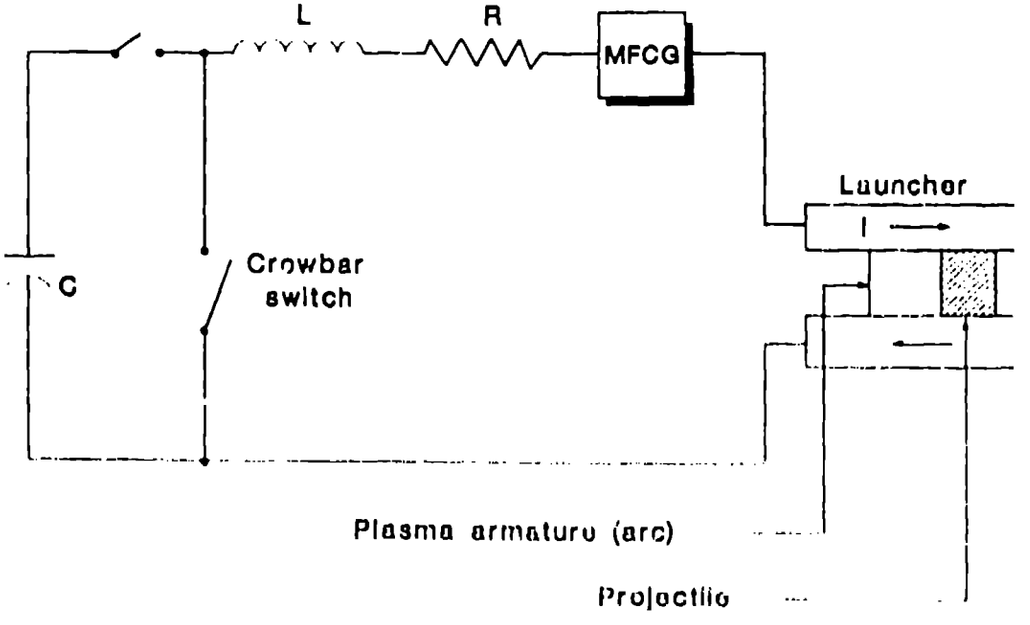

Fig. 1. Schematic diagram of a railgun

armature. The armature, in turn, exerts a force on the projectile causing a rapid acceleration.

A study of railguns has been in progress at Los Alamos since 1978. Although the work has been primarily experimental, a significant effort has also gone into developing extensive analytical capabilities. A series of codes has been developed to predict electrical, dynamic, structural, and thermal effects in a railgun system.

In the current railgun program, Los Alamos is designing and constructing the Lethality Test System (LTS), which has the goal of accelerating 20- to 30-g projectiles to velocities of 15 km/s. This paper describes the codes used to predict EML system performance and presents results specific to the LTS design. Numerical predictions are compared with experimental data and presented for the LTS low-pressure prototype.

ANALYTICAL CAPABILITIES

Figure 2 shows the interrelationships between the codes used for railgun analysis. In the initial step in a system analysis, the FLD code is used to

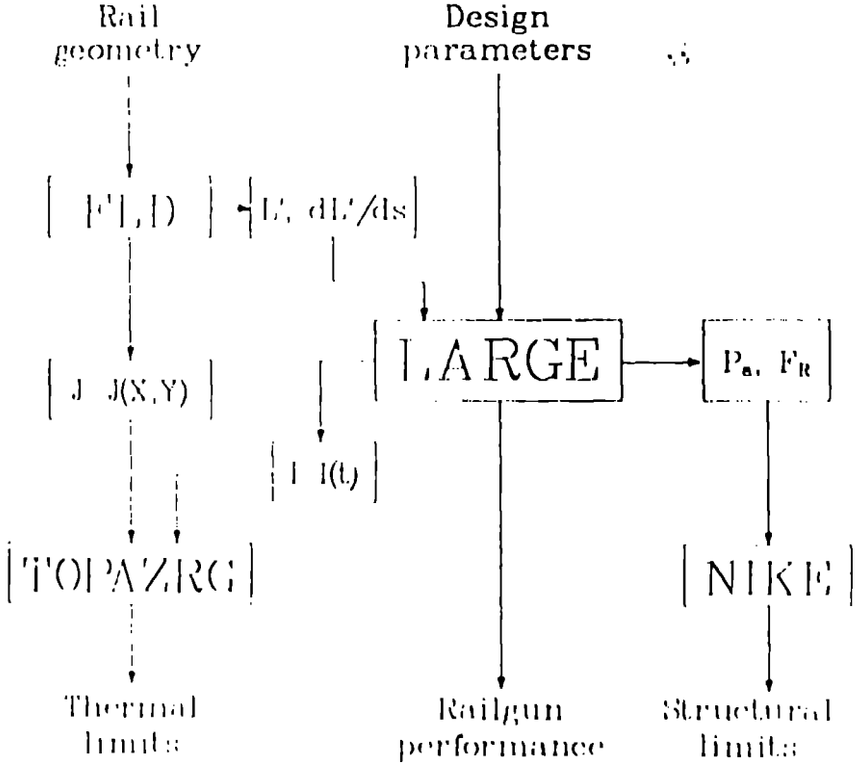

Fig. 2. Interrelationships among codes used for railgun analysis.

determine the inductance gradient, L', and the derivative of the inductance gradient with respect to rail spacing, dL'/ds, for the proposed launcher. The distribution of current density around the perimeter of the rail, J(x,y), is also calculated. The inductance gradient and its derivative are used as input to the LARGE code, along with such design parameters as rail geometry, mass and injection velocity of the projectile, and power supply specifications. Parametric studies may be performed to determine projectile velocity for a range of design parameters. Additional results computed by LARGE include the rail current as a function of time, I(t), and the pressure, P_a, and magnetic force, F_r, acting on the rails. These parameters are used as input to the thermal analysis code, TOPAZRG, and the structural analysis code, NIKE2D. These codes are used to ensure that the thermal and structural limits of the system are not exceeded. Each code is described in more detail in the remainder of this section.

FLD Inductance Gradient Calculations

The FLD code [3] is used to calculate the current density distribution, magnetic field, and inductance of long, parallel conductors of arbitrary cross sections in the high-frequency limit. These results may be used for railguns as initial values, which are applicable until the current or magnetic field diffusion has significantly changed the current distribution. The method used here follows from the equivalence of the current distribution problem to the problem of charge distribution on equipotential (electrostatic) surfaces [4]. The axial component of the magnetic vector potential is equivalent to the electrostatic potential. The first step in the calculation is to find the current distribution that produces a constant value of the vector potential on each conductor surface. An existing computer program was used for these calculations [5]. The values of the magnetic vector potential on each conductor surface are determined by the total flow of current in the circuit and the geometric symmetry of the conductors. Once the current distribution is known, the magnetic field associated with the conductors can be calculated. In particular, the total flux that links the circuit can be determined from the field between the rails. The self inductance of the circuit is easily calculated from the total flux linkage.

A series of calculations was performed to determine inductance gradients and current distributions for the LTS rails. The geometry of the LTS rail and support structure (anvil) is shown in Fig. 3. The bore radius is R = 12.5 mm. The effects of rail thickness, W, and anvil location, X_1, on the inductance gradient and the derivative of inductance gradient with respect to rail spacing are shown in Figs. 4 and 5. These results indicate that both L' and dL'/ds increase with increasing X_1 and decreasing rail thickness. The Lorentz force accelerating the armature is proportional to L', and thus L' should be as large as possible. Because the force tending to spread the rails apart is proportional to dL'/ds and must be kept small enough to prevent structural damage, a tradeoff is required in the selection of rail and anvil geometry. The geometric parameters selected, based largely on structural considerations, were W = 14.53 mm and X_1 = 106.4 mm

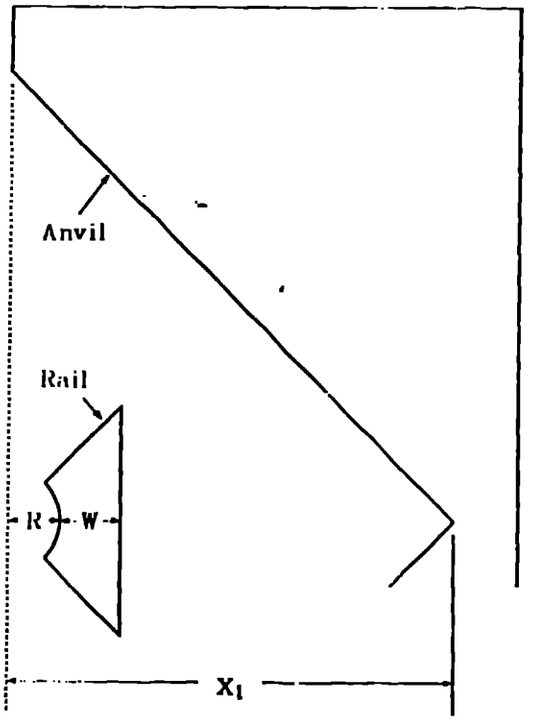

Fig. 3. Geometry of the LTS launcher.

The instantaneous relative current density distribution on the surface of the LTS rail is shown in Fig. 6. The zero value of arc length is at the center point of the bore (curved surface), and arc length is measured along the perimeter in the clockwise direction. Because of symmetry about the x axis, results are shown for only the top half of the rail. The peaks represent the current densities at the corners of the rail. The current density would be unbounded for sharp corners. It is therefore necessary to specify a radius of curvature at the corners. The values selected here were 0.13 mm and 0.54 mm for the front and back corners respectively. The peaks in Fig. 6 can be reduced by using larger radii or curvature.

LARGE EML Performance Predictions

The Los Alamos Rail Gun Estimator (LARGE) is a performance model that was written to calculate rail current and projectile velocity and position from a description of the power supply and railgun [6]. It can model a capacitor bank, large inductances in the power supply; explosively driven magnetic flux compression generators (MFCGs); various railgun configurations such as square bore or round bore, staged systems; or distributed systems. All rail inductances and resistances are calculated from a physical description of the rails. The rail inductance gradient (high frequency limit) calculated by FFD, is used to determine the force on the projectile. Estimates of how current diffusion changes rail inductance and resistance with time are also included [7].

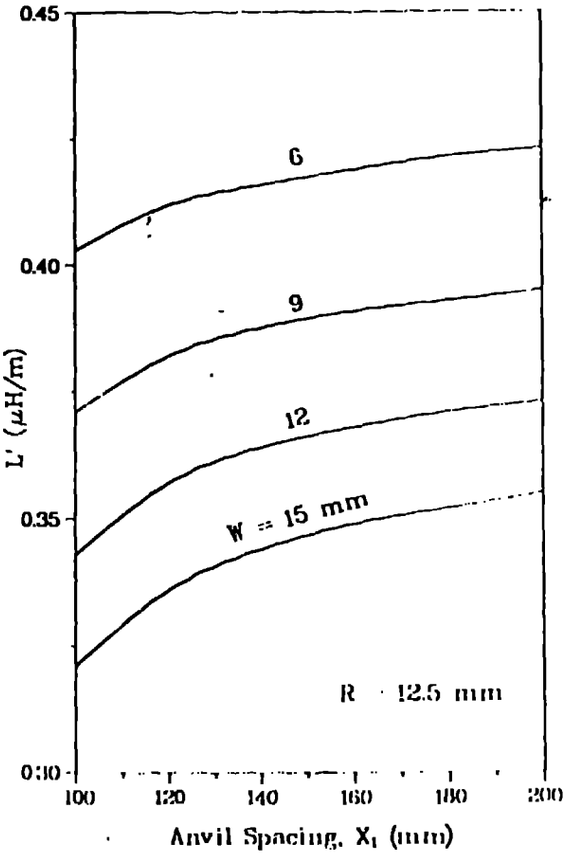

Fig. 4. Inductance gradients calculated by the FLD code for the LTS.

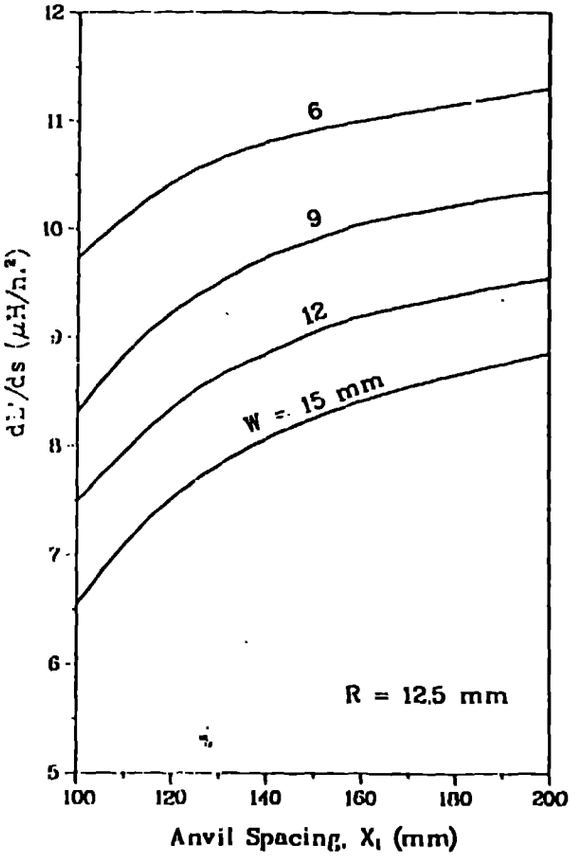

Fig. 5. Derivatives of inductance gradients calculated by the FLD code for the LTS.

One of the most important losses in plasma-armature railguns is caused by ablation of the rail and insulator material [8,9]. The radiant heat flux from the arc is so large that surface material can be vaporized and ionized within a few microseconds. The resulting material may be entrained in the arc. This causes an increase in the total mass that must be accelerated and a lower muzzle velocity. The increased size of the arc also causes an increase in arc drag [10]. An algorithm is included in LARGE which estimates the rate of ablation and computes the resulting arc mass and arc drag.

The LARGE code uses an explicit marching procedure so that parameters calculated at the end of a time step are based on conditions at the beginning of the time step. First, the rail current is computed by simultaneously solving the circuit equations for all stages. This is done numerically using Euler's method. The current is then used to compute Joule heating in the arc, and an energy balance is used to calculate ablation rates and changes in the mass and in the arc length. Finally, the

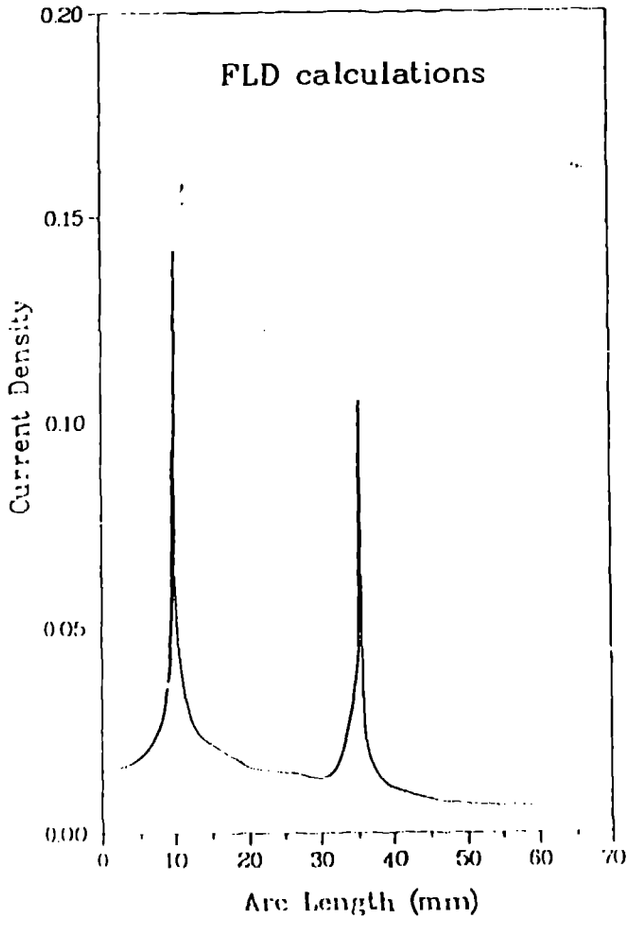

Fig. 6. Instantaneous relative current density distribution for the LTS rail calculated by the FLD code.

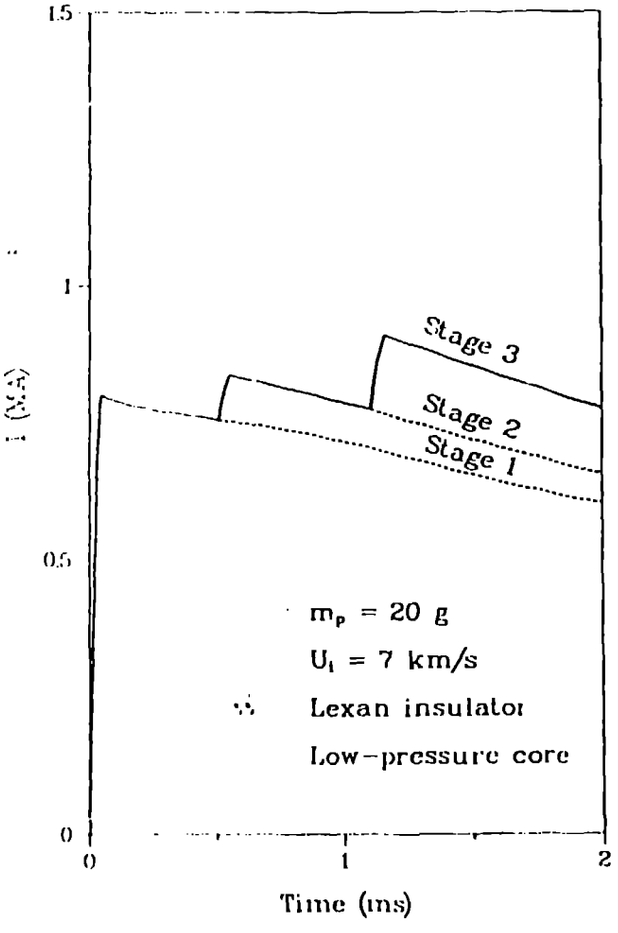

Fig. 7. Rail current profile for the LTS computed by the LARGE code.

conservation of energy principle applied to the arc and projectile is used to compute the acceleration, velocity, and displacement of the projectile.

The LARGE code was used to predict the performance of the LTS system. Results are shown in Figs. 7 and 8 for the case of the low pressure core. The power supply parameters were adjusted so that the arc pressure would not exceed 30 ksi at any time during the launch. The projectile mass and initial velocity were specified as 20 g and 7 km/s. Electrical leads for the three stages were located at 0, 4, and 10 m from the breech.

The solid line in Fig. 7 represents the arc current. The dashed lines represent the current in the first and second stages. The rise time for each stage was 50 μs. The velocity vs time plot (Fig. 8) indicates a muzzle

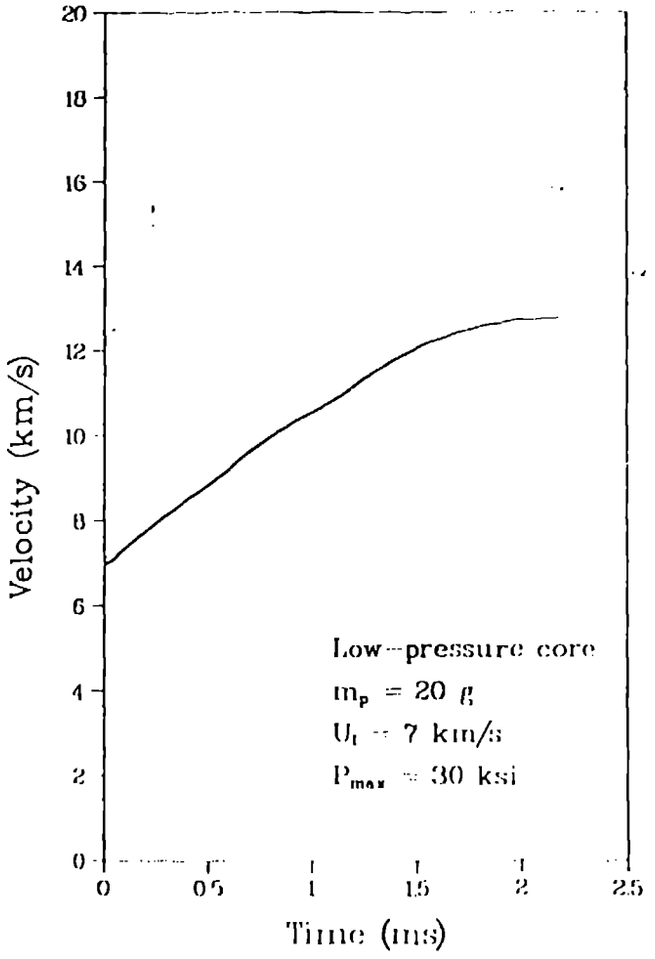

Fig. 8. Projectile velocities predicted by LARGE

velocity of 12.5 km/s. Velocities well above 15 km/s are predicted for the high-pressure core where higher rail currents cause higher accelerations of the projectile.

Some preliminary experiments have been completed using a prototype of the low-pressure LTS. The rails for the prototype are 3.66-m long, and a 1.88-MJ capacitor bank was used instead of the 50 MJ power supply that will be available for the full LTS. LARGE simulations were performed to check the accuracy of the code. A comparison of the numerical and experimental results is shown in Fig. 9. Current profiles were measured for each experiment, then the current vs time profiles were used as input to LARGE and the rail current calculations were bypassed. The differences between the numerical and experimental results are therefore primarily an indication of the accuracy of the ablation and arc drag algorithms. Note that in some cases two different current profiles were used. The breech current was measured just downstream of the electrical lead for this single-stage experiment. In some cases current measurements at a series of locations along the rail indicated that the plasma arc split into two segments after traveling some distance down the bore. The resulting data were used to infer a minimum effective current profile. That profile neglected any effect that the current in the trailing arc might have in producing a force that could be transmitted to the projectile. Simulations were also performed in which the effects of ablation and arc drag were omitted. These simulations are the ideal cases (solid points) shown in Fig. 9. Agreement between the numerical and experimental results is quite good. The numerical results for the ideal calculations significantly overpredict muzzle velocities. These results as well as other simulations discussed in Refs. 9 and 10 indicate that ablation and arc drag are important loss mechanisms and that the LARGE code is able to predict the performance of a wide variety of railgun systems.

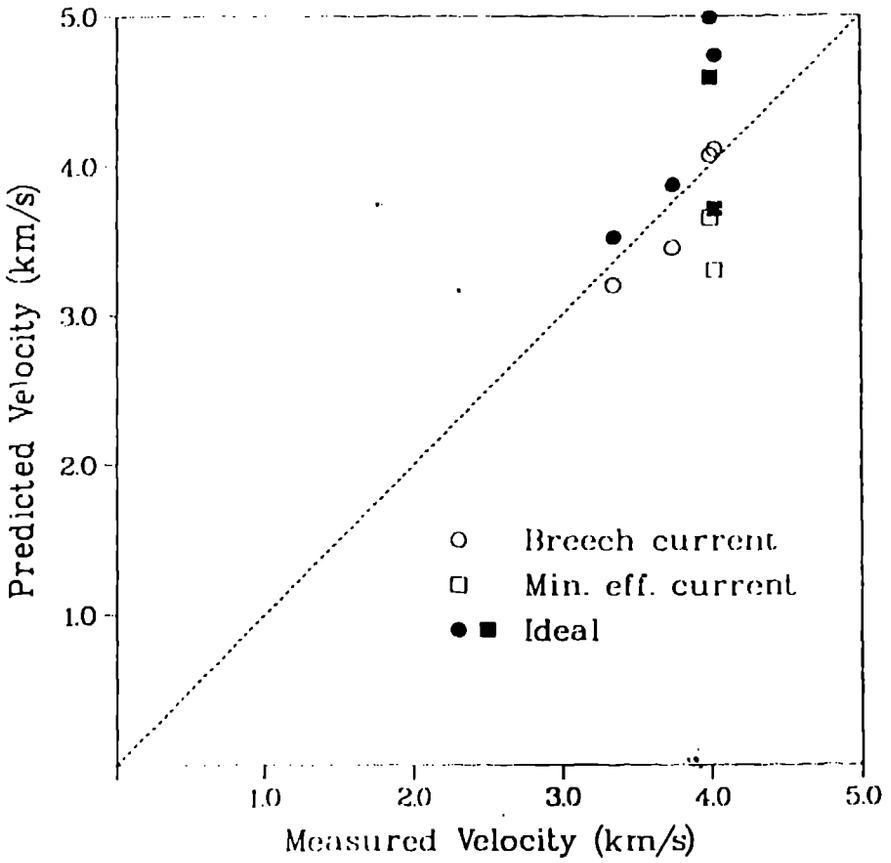

Fig. 9. A comparison of predicted and measured velocities for the LTS Low-Pressure Prototype.

TOPAZRG - Thermal Analysis

Thermal analysis of the rails was performed using the TOPAZRG [11] code, a two-dimensional, transient, finite-element code that solves the combined thermal/electrical field diffusion problem for the rails. The current profile (Fig. 7) and surface current density distribution (Fig. 6) were used as input along with specification of magnitude and duration of arc radiation impinging on the bore surface of the rails.

Thermal analyses were performed using TOPAZRG for segments of rail at the breech and at a small distance downstream from the third stage electrical connections. Results for the TOPAZRG calculations at the breech are shown in Fig. 10. The arc radiation was assigned a magnitude of 1.0 MW/cm^2 (an effective average arc temperature of approximately 20,000 K) and a duration of 10 μs. This corresponds to a 7 cm long arc moving at a velocity of 7000 m/s. Note that the temperature at the inside corner of the rail increases very rapidly to a temperature near the melting point. Temperatures along the bore surface have similar but slightly lower peaks because the Joule heating is less severe at points farther removed from the corner. The

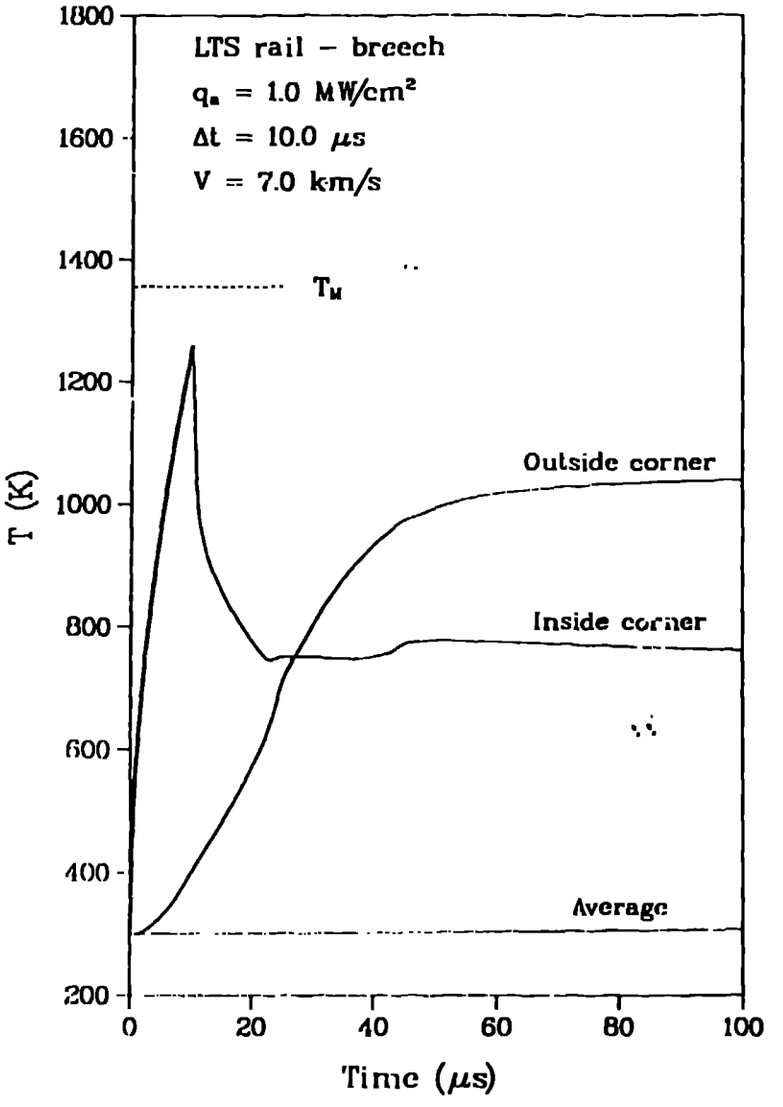

Fig. 10. Temperature profiles at the breech calculated by TOPAZRG.

temperature drops rapidly after the 10 μs radiant energy pulse because of thermal diffusion, then begins to rise again as the Joule heating increases. The first stage current has a rise time of 50 μs, after which the rate of temperature increase drops somewhat as the rail current begins to decrease. Thermal diffusion finally causes the temperature at the inside corner to decrease after about 150 μs (not shown). Note that the temperature at the back corner is virtually unaffected by the radiant flux because the rail thickness is large compared with the the thermal diffusion depth for the time scale of this simulation.

A simulation was also performed for a rail segment where the third-stage leads are connected because the maximum current occurs at that location. For that case, time was measured from the instant the projectile reached that location. The current was assumed to rise linearly from zero to the maximum value of Fig. 7 in the time it took the arc to pass. For this simulation, a value of 10 μs was used. This corresponds to a 12-cm-long arc moving at a velocity (calculated by LARGE) of 12 km/s. The larger and more rapid contribution of Joule heating for this case caused the predicted temperature at the inside corner to exceed the melting temperature of copper. Note that the temperature at the outside corner also exceeds the melting temperature.

The calculations described above assumed a single-phase material. They overpredict temperatures above the melting temperature because the absorption of energy that occurs with phase change is neglected. The TOPAZ2D code includes a phase-change algorithm so that the effects of melting can be assessed. Results of the calculations for the rail segment downstream of the third stage, including the phase-change algorithm, indicated temperatures with peaks approximately 150 K lower than those shown in Fig. 11. The corner temperatures also dropped below the melting temperature somewhat more rapidly. The inclusion of the phase-change algorithm has an extremely negative impact on computational speed. The number of iterations required at each time step increases dramatically because of the strong nonlinearities introduced by phase change. The time step required to maintain stability is limited to approximately 0.2 μs. The computation for 20 μs using 400 elements required more than 15 min. of central processing unit (CPU) time on the Cray. The calculation that does not include melting is more than ten times faster.

It should be noted that corner temperatures somewhat above the melting point are not likely to cause severe problems. Temperatures at nodes adjacent to the corner nodes remained well below the melting temperature in most cases, so the high temperature region is extremely localized. The corner temperatures began to decrease because of thermal diffusion shortly after the arc had passed and the rail current had begun to decrease. They typically drop below the melting temperature within 1 to 2 ms. A small amount of melting at the outside corner of the rail is not expected to cause serious problems because the rail is surrounded by insulator material and has little room to deform. Only a small deformation is expected at the inside corner because the forces acting on the material there are primarily radially outward. They include the arc pressure (estimated to be in the range of 30 to 50 ksi) and the magnetic forces that tend to spread the rails apart.

NIKE2D Structural Analysis

The structural analysis was performed using the NIKE2D [12] code. This is an implicit finite element code for analyzing static and dynamic response of two dimensional solids. Of the many material models available in NIKE2D, the elastic, elastic plastic, orthotropic and thermo orthotropic were used for this analysis. The contact algorithm (slideline) in NIKE2D is useful

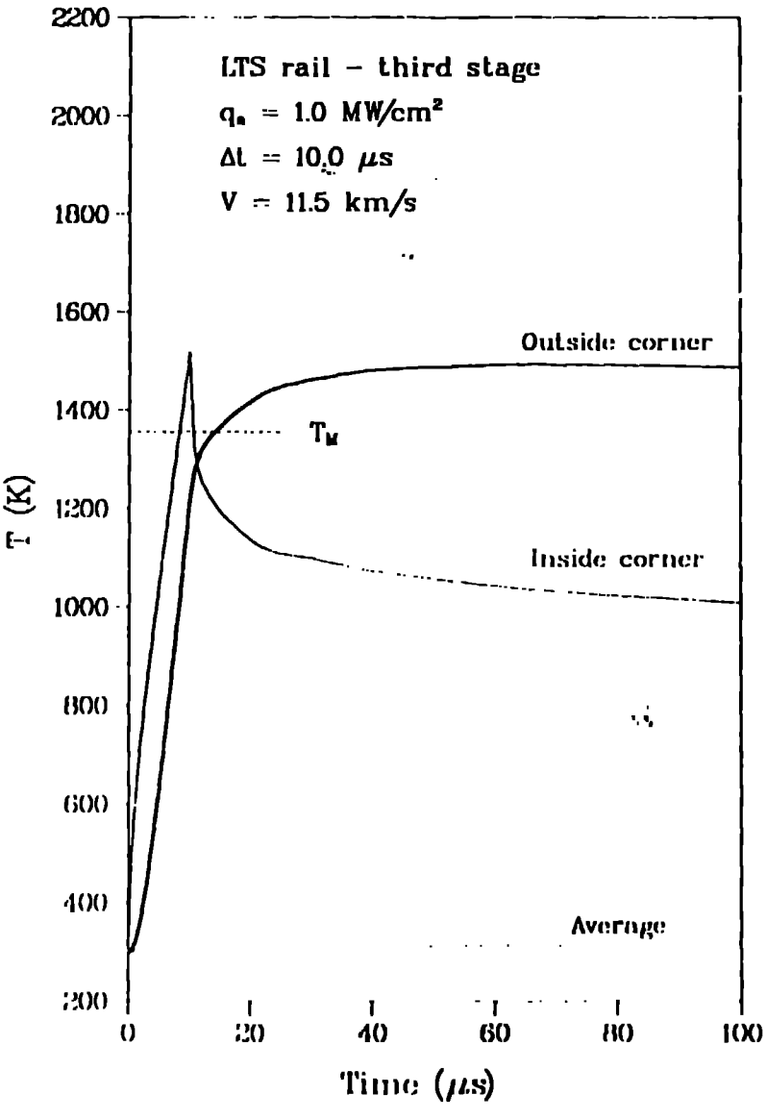

Fig. 11. Temperature profiles at the third stage calculated by TOPAZRG.

for railgun problems. The ability to calculate thermal stresses was used in an artificial manner for the preload analysis. The meshes for these calculations were generated using INGEN [13] and ISCHEK [14]. The results were examined graphically with STRAPP [15] and TOAP [16].

For this analysis, the plane strain geometry assumption was made. Therefore, variations in the loading and structural response along the length of the launcher were not considered. The model is shown in Fig. 12.

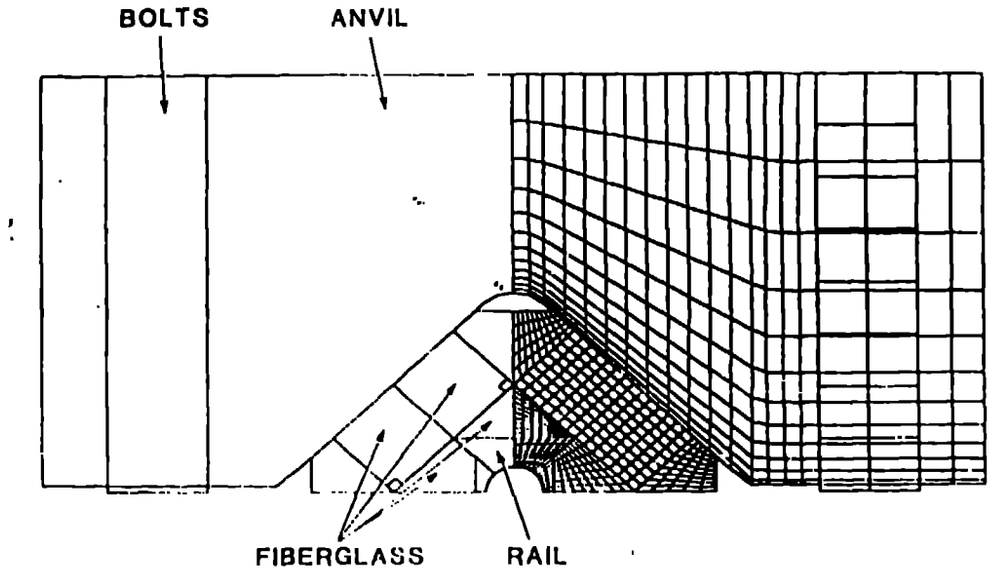

Fig. 12. LTS low-pressure core - FEM model.

Slidelines were used extensively to define the interactions between the various launcher components. The bolt preload was applied by artifically cooling the bolts until the correct (measured) preload was obtained. The dynamic loads on a launcher under firing conditions (the plasma pressure and rail force) were applied to the preload model. Thus, stresses and motions were determined resulting from the combined application of preload and firing loads. These analyses are described in more detail in Ref. 17.

The firing loads were determined at a critical longitudinal cross section by considering the arc current passing the point. The arc current and arc length were either determined by LARGE or taken from experimental data (Fig. 7). The inductance gradients necessary to determine plasma pressure and rail force were determined by FLD calculations (Figs. 4 and 5). Figure 13 shows the loading functions that occurred at the longitudinal cross section that contained the second current probe in Test 6 of the LTS low pressure core prototype. This location corresponds to the longitudinal location of the arc when peak current was reached.

The rise time of the plasma pressure is assumed to be the time required for the projectile to pass the second current probe location. The plasma pressure decayed to zero when the tail of the arc passed. The rail force increased to a peak when the end of the arc passed. Note that the peak pressure and peak rail force did not occur at the same time. The pressure load was applied to the inner surface of the bore, both to the rail and to the insulator (side wall). The rail force was distributed around the surface of the rail in a manner similar to the actual magnetic force distribution.

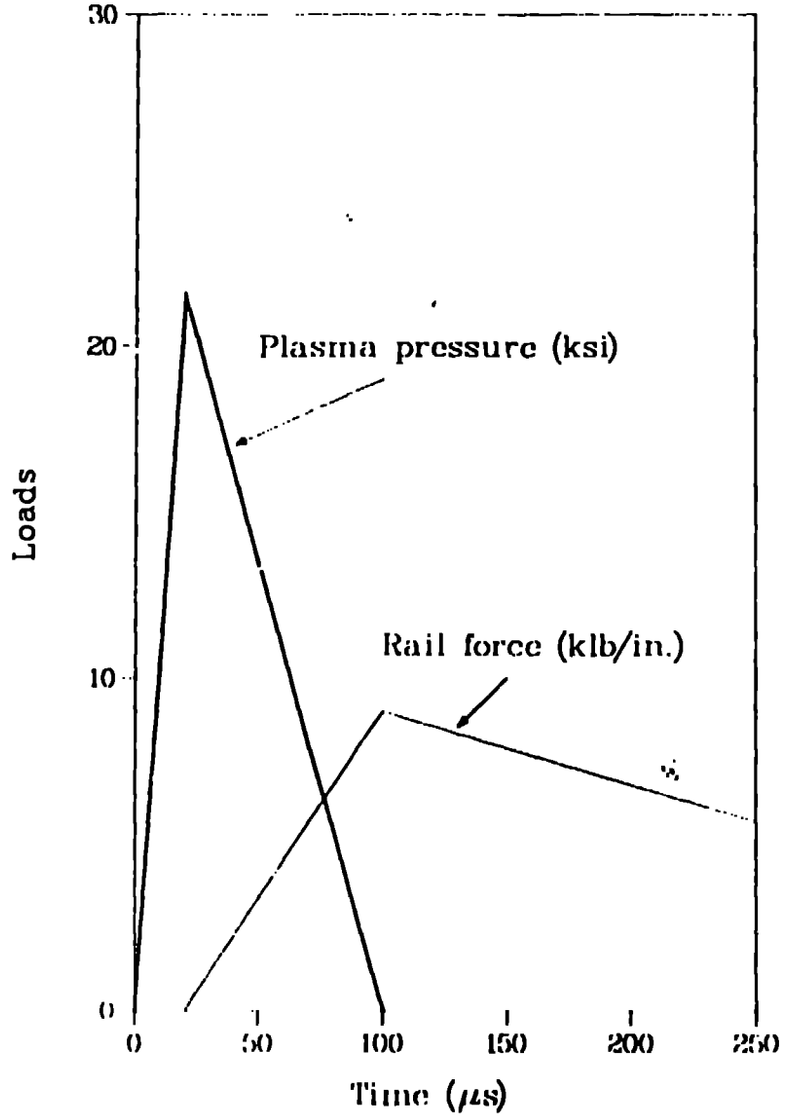

Fig. 13 Loads on CIS low pressure prototype test 6

The structural analysis results yielded a wealth of information which we don't have space to discuss here. The results allowed prediction of the bolt preload, the stresses in internal components, and the interface gaps. Based on this information, the performance of the launcher was characterized and several design modifications were made. As an example of the analytical results, Fig. 14 shows the rail displacement as a function of time indicating a calculated peak deflection of 17 mils.

As an indicator of the accuracy of the structural analysis, Fig. 14 also shows the test data for the rail motion. The peak displacement was predicted with reasonable accuracy (17 mils predicted and 19 mils measured) The initial rail pinching (negative deflection at 340 μs) shown in the data does not show up in the analysis because rail pinching is caused by a

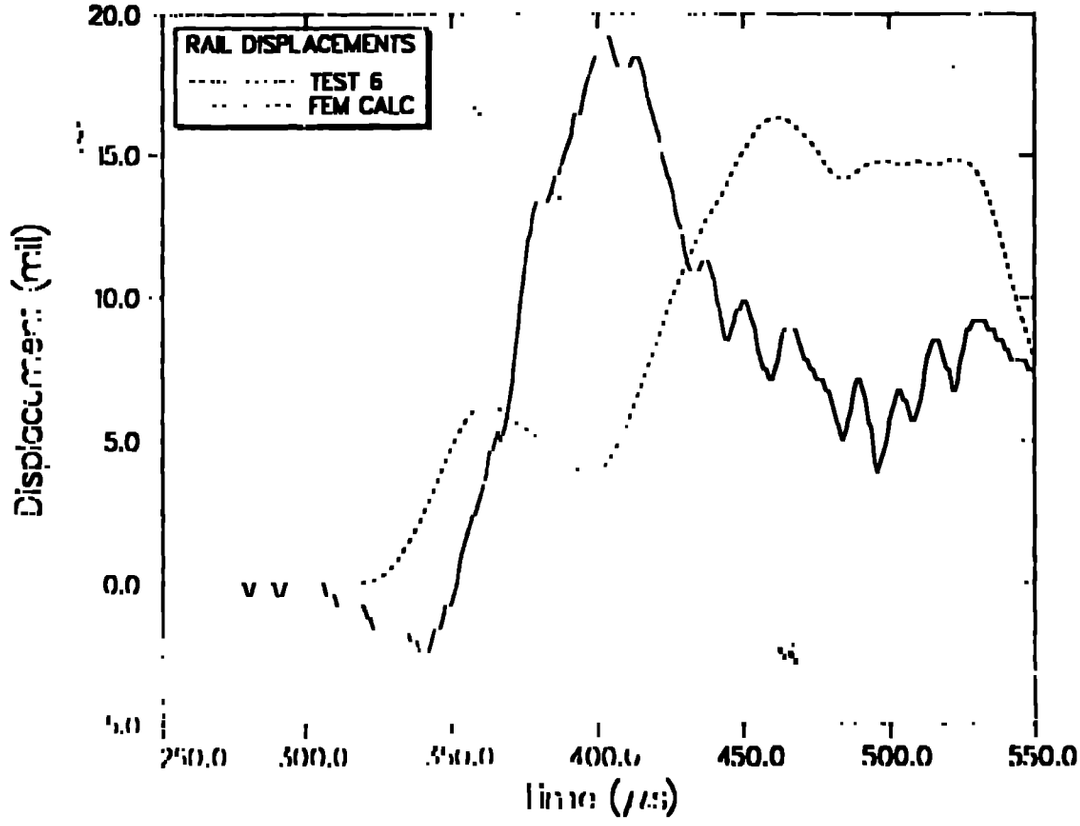

Fig. 14. Rail motion for TIS low pressure core prototype Test 6.

longitudinal load variation that is not considered in this two dimensional analysis. The difference in rise time and general response shape are probably due, at least partly, to uncertainties in the arc length used for the calculation. The accuracy of the calculated displacement history is certainly sufficient for design purposes.

SUMMARY

A series of computer codes has been developed to perform a complete analysis of EM systems. Analytical capabilities include detailed structural and thermal analysis of the launcher as well as performance simulations of the entire system. These codes have been instrumental in the design of the EM at Los Alamos. Comparisons of analytical predictions with experimental results obtained for the EM low pressure prototype have shown generally good agreement.

ACKNOWLEDGMENTS

The authors wish to thank J. V. Parker and W. A. Cook for their technical support and M. M. Plehn and L. L. Shelley for their word processing and editorial assistance.

REFERENCES

1. R. A. Marshall, "The Australian National University Rail Gun Project," *Atomic Energy in Australia*, 18, 16-18 (1975).

2. S. C. Rashleigh and R. A. Marshall, "Electromagnetic Acceleration of Macroparticles to High Velocities," *J. Appl. Phys.* 49, 2540-2542.

3. J. F. Kerrisk, "Current Distribution and Inductance Calculations for Rail-Gun Conductors," Los Alamos National Laboratory report LA-9092-MS (October 1981).

4. H. R. Lewis, Jr., "Computation of Electrostatic and Rapidly Pulsed Magnetic Fields," *J. Appl. Phys.* 37, 2541-2550 (1966).

5. K. R. Crandall, "Computation of Charge Distribution on or Near Equipotential Surfaces," Los Alamos Scientific Laboratory report LA-3512 (December, 1966).

6. J. F. Kerrisk, "Electrical and Thermal Modeling of Railguns," IEEE Transactions on Magnetics, Vol. MAG-20, 399-402 (March 1984).

7. J. F. Kerrisk, "Current Diffusion in Railgun Conductors," Los Alamos National Laboratory report LA-9401-MS (June 1982).

8. J. V. Parker, "Performance Loss due to Wall Ablation in Plasma Armature Railguns," presented at AIAA 18th Fluid Dynamics and Plasmadynamics and Laser Conference, Cincinnatti, Ohio, (July 16-18, 1985).

9. N. M. Schnurr and J. F. Kerrisk, "Numerical Studies of Ablation and Ionization of Railgun Materials," presented at the AIAA 18th Fluid Dynamics and Plasmadynamics and Laser Conference, Cincinnatti, Ohio (July 16-18, 1985).

10. N. M. Schnurr, J. F. Kerrisk, and J. V. Parker, "Numerical Predictions of Railgun Performance Including the Effects of Ablation and Arc Drag," in Proceedings of the 3rd Symposium on Electromagnetic Launch Technology, Sprit AI-24, 1986, Austin, Texas, pp. 271-278.

11. N. M. Schnurr, "Thermal Analysis of Electromagnetic Launcher Rails," Los Alamos National Laboratory report in progress.

12. J. O. Hallqu st 'NIKE2D - A Vectorized. Implicit. Finite Deformation Finite Element Code for Analyzing the Static and Dynamic Response of 2-D Solids with Interactive Rezoning and Graphics, "Lawrence Livermore National Laboratory report UCID-19677. Rev. 1, December. 1986.

13. W. A. Cook. INGEN: A General Purpose Mesh Generator for Finite Element Codes." Los Alamos National Laboratory report LA-9402-MS (June 1982).

14. W. R. Oakes. Jr.. "ESCHER User's Manual," Los Alamos National Laboratory report (in progress)

15. F M. Guerra. "STRAPP User's Manual." Los Alamos National Laboratory report (in progress).

16. W. D. Birchler and B. M. Wheat. "TDAP User s Manual." Los Alamos National Laboratory internal report. 1985.

17. R. F. Davidson et al . "Predicting Bore Deformations and Launcher Stresses in Railguns." in Proceedings of the 3rd Symposium on Electromagnetic Launch Technology. April 21-24. 1986. Austin. Texas. pp. 31-36.